MC5R Contributes to Sensitivity to UVB Waves and Barrier Function in Mouse Epidermis

Akari Shintani[1], Hiromi Sakata-Haga[1], Keiichi Moriguchi[2], Mitsuhiro Tomosugi[1], Daisuke Sakai[3], Tsuyoshi Tsukada[1], Makoto Taniguchi[4], Masahide Asano[5,6], Hiroki Shimada[7], Hiroki Otani[8], Hiroki Shoji[3], Junko Hatta[9], Takashi Mochizuki[9] and Toshihisa Hatta[1]

MC5R is known for its role in the exocrine function of sebaceous glands, but other functions in the epidermis remain unclear. This study focused on the relationship between MC5R and homeostasis in the epidermis and examined the role of MC5R in mice whose skin was irradiated with UVB waves. UVB irradiation-induced skin ulcers and severe inflammation at lower doses in homozygotes of *MC5R*-deficient (i.e., $MC5R^{-/-}$) mice (150 mJ/cm^2) than the doses in wild-type mice (500 mJ/cm^2). Transepidermal water loss was increased (approximately 10-fold) in adult $MC5R^{-/-}$ mice compared with that in wild-type mice. In neonates, a dye exclusion assay showed no remarkable difference between $MC5R^{-/-}$ and wild-type mice. After UVB irradiation, compared with wild-type mice, $MC5R^{-/-}$ mice showed increased inflammatory cell infiltration in the dermis of the ulcerative region, significantly increased thickness of the epidermis in the nonulcerative region, significantly more prickle cells in the nonulcerative region, and increased serum IL-6 levels but decreased IL-10 levels. Transmission electron microscopy revealed fewer lamellar granules, less lipid secretion, and an expansion of the *trans*-Golgi network in the epidermis in $MC5R^{-/-}$ mice. This study elucidated the increased sensitivity to UVB irradiation and decreased barrier function in $MC5R^{-/-}$mice.

JID Innovations (2021);**1:**100024 doi:10.1016/j.xjidi.2021.100024

INTRODUCTION

ACTH and melanocyte-stimulating hormones (α-, β-, and γ-melanocyte–stimulating hormones), called melanocortin, are transcripts of the *POMC* gene and are produced by post-translational modification. They are known as endogenous agonists of melanocortin receptors. The five melanocortin receptor subtypes—MC1R to MC5R—each have different tissue expression patterns and unique profiles for the relative potency of different melanocortin peptides (Simamura et al., 2011; Zhu et al., 2019). Whereas MC1R is involved in skin pigmentation, MC2R is involved in steroid secretion and only mediates the action of ACTH, and MC3R and MC4R regulate energy homeostasis in the CNS (Cone, 2006). Cloned from human genomic DNA by homology screening in 1993 and from the mouse genome the following year, MC5R was the last member of the melanocortin gene family to be cloned (Gantz et al., 1993). MC5R has the same ligand recognition affinity as MC1R and MC4R, whose strongest ligand is α-melanocyte–stimulating hormone (Catania et al., 2004). MC5R is expressed in many tissues, such as adrenal glands, exocrine glands, skin, lymph nodes, and so forth.

In normal skin, MC5R is highly expressed in the apocrine and eccrine glands, sebaceous glands, epidermal keratinocytes (KCs), and dermal migrating cells (Hatta et al., 2001; Lovászi et al., 2017; Thiboutot et al., 2000; Zhang et al., 2011). MC5R-deficient homozygote ($MC5R^{-/-}$) mice showed impairment of the exocrine function (van der Kraan et al., 1998) and reduced sebum production, resulting in functional deterioration of water repulsion and thermoregulation (Chen et al., 1997), with the exocrine effects of MC5R on the skin having been well characterized, but the role of MC5R in the KCs of the epidermis, where it is also expressed, has not yet been elucidated. The skin fulfills the physiological barrier function of maintaining and protecting the organism. However, the skin barrier function involving the sebaceous membrane due to decreased sebum has not been evaluated in $MC5R^{-/-}$ mice. In this study, the role of MC5R in the epidermis was analyzed from both the skin barrier function and the maintenance of the skin cells in inflammation using $MC5R^{-/-}$ mice irradiated with UVB.

RESULTS

Histological analysis of the epidermis

Expression of MC5R was observed in KCs, sebaceous glands, and migrating cells in the dermis of wild-type (WT) mice but

[1]*Department of Anatomy, School of Medicine, Kanazawa Medical University, Uchinada, Japan;* [2]*Department of Oral Anatomy, School of Dentistry, Aichi Gakuin University, Nagoya, Aichi, Japan;* [3]*Department of Biology, Kanazawa Medical University, Uchinada, Japan;* [4]*Department of Life Science, Medical Research Institute, Kanazawa Medical University, Uchinada, Japan;* [5]*Institute of Laboratory Animals, Graduate School of Medicine, Kyoto University, Kyoto, Japan;* [6]*Division of Transgenic Animal Science, Advanced Science Research Center, Kanazawa University, Kanazawa, Japan;* [7]*Department of Medical Science, School of Nursing, Kanazawa Medical University, Uchinada, Japan;* [8]*Department of Developmental Biology, Faculty of Medicine, Shimane University, Izumo, Japan; and* [9]*Department of Dermatology, School of Medicine, Kanazawa Medical University, Uchinada, Japan*

Correspondence: Toshihisa Hatta, Department of Anatomy, School of Medicine, Kanazawa Medical University, 1-1 Daigaku, Uchinada, Kahoku-gun, Ishikawa 920-0293, Japan. E-mail: thatta@kanazawa-med.ac.jp

Abbreviations: KC, keratinocyte; SG, stratum granulosum; TEM, transmission electron microscopy; TEWL, transepidermal water loss; TGN, trans-Golgi network; TLC, thin-layer chromatography; WT, wild type

Received 26 November 2020; revised 23 March 2021; accepted 5 April 2021; accepted manuscript published online XXX; corrected proof published online XXX

Cite this article as: JID Innovations 2021;1:100024

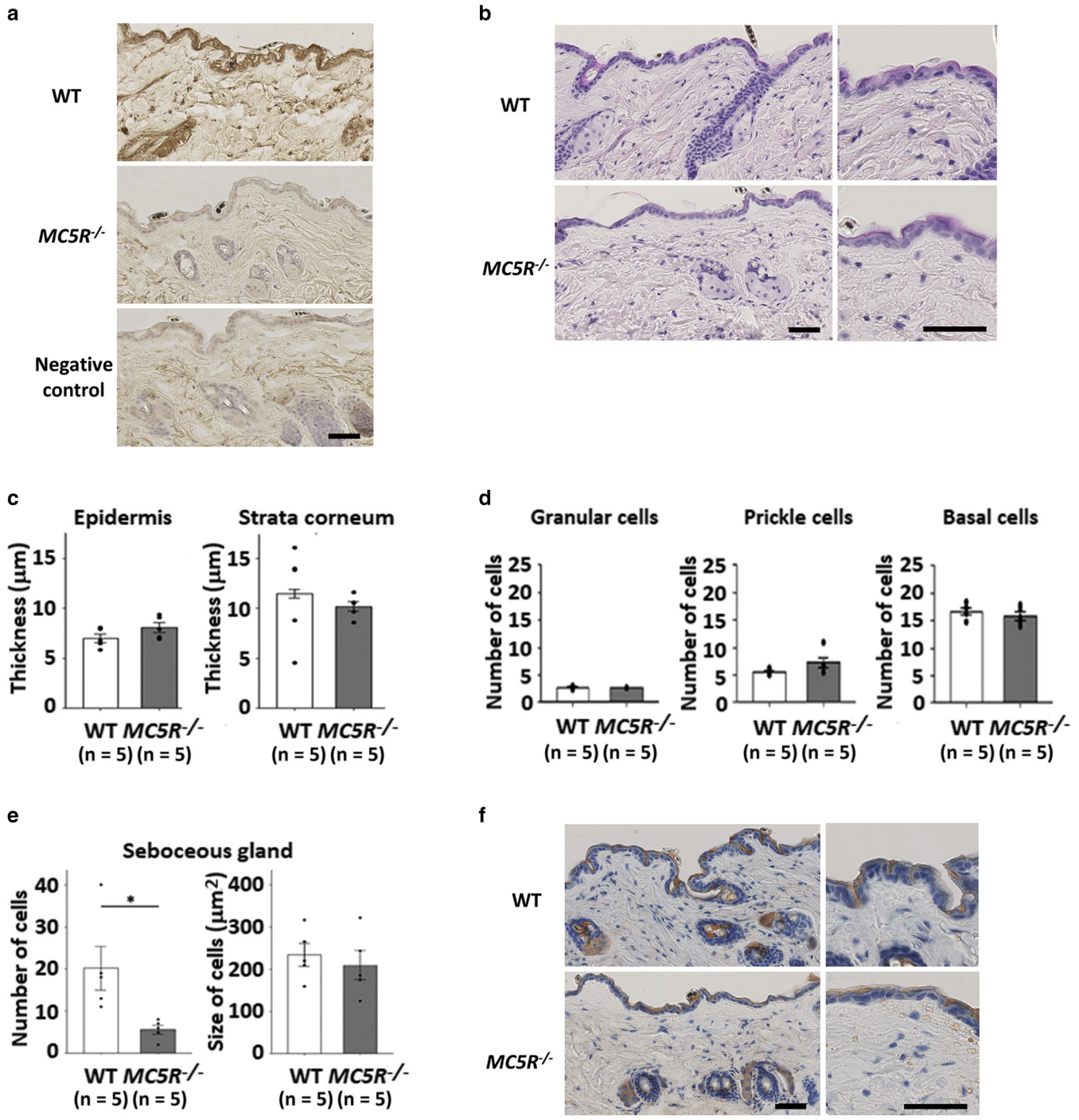

Figure 1. Histological difference in the skin between *MC5R*$^{-/-}$ and WT mice before UVB irradiation. (**a**) MC5R immunostaining in the epidermis. (**b**) The histology of epidermis with H&E staining. (**c, d**) The thickness of the epidermis and stratum corneum and the number of cells in each layer. (**e**) The number of sebaceous gland cells. (**f**) Sudan III staining for sebaceous membrane. Data are expressed as mean ± SEM. *$P < 0.05$. WT mice, $n = 5$; *MC5R*$^{-/-}$ mice, $n = 5$. Bar = 100 μm. WT, wild type.

not in that of *MC5R*$^{-/-}$ mice (Figure 1a). A histological examination revealed no significant differences in the structure or thickness of the epidermis and stratum corneum and in the number of cells from the stratum basal to the stratum corneum between WT and *MC5R*$^{-/-}$ mice (Figure 1b–d). Although the area of cross-sections in the sebum cells did not differ significantly between the WT and *MC5R*$^{-/-}$ mice (Figure 1e), the number of sebum cells was significantly lower in *MC5R*$^{-/-}$ than in WT mice ($P < 0.05$). Sudan III staining showed the sebum membranes in both WT and *MC5R*$^{-/-}$ mice, but no clear difference was detected between the groups (Figure 1f).

Effects of UVB irradiation on *MC5R*$^{-/-}$ mice

The association between the UVB irradiation dose and the amount of skin damage was examined 7 days after

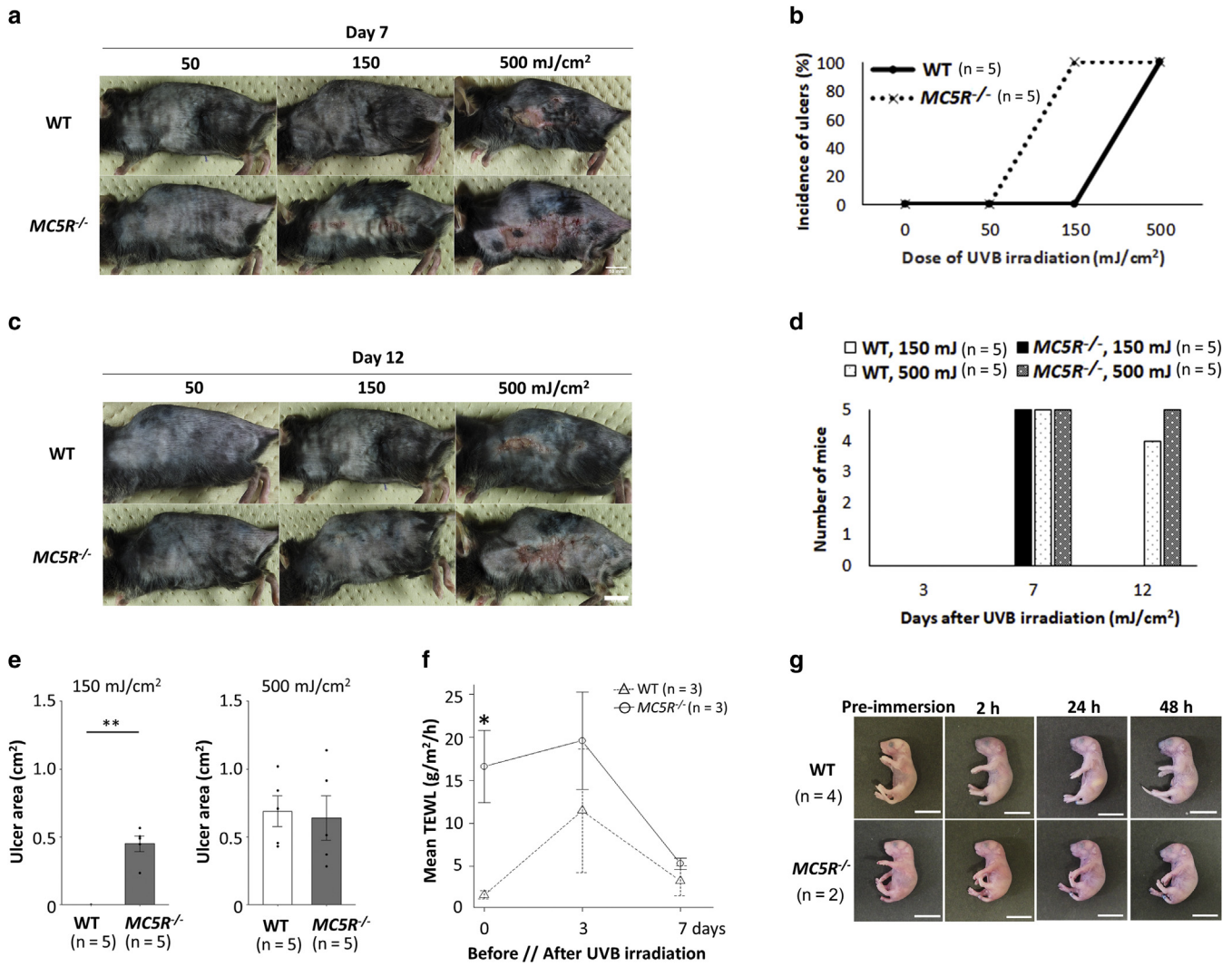

Figure 2. Chronological changes in the skin after irradiation. (**a, b**) Ulceration was observed after irradiation of 150 and 500 mJ/cm^2 in *MC5R*$^{-/-}$ mice and only after irradiation of 500 mJ/cm^2 in WT. (**c**) Skin ulcers in both groups with irradiation at 500 mJ/cm^2. (**d**) Incidence rates of skin ulcers. (**e**) Ulcer area 7 days after irradiation. Data are presented as mean ± SEM. $^{**}P < 0.01$. WT mice, $n = 5$; *MC5R*$^{-/-}$ mice, $n = 5$. (**f**) TEWL was measured on nonulcer skin. $^{*}P < 0.05$. WT mice, $n = 3$; *MC5R*$^{-/-}$ mice, $n = 3$. (**g**) Dye exclusion assay showed no remarkable difference. WT mice, $n = 4$; *MC5R*$^{-/-}$ mice, $n = 2$. Bar = 1 cm. The nonulcerated area is not a healed ulcerated area. TWEL, transepidermal water loss; WT, wild type.

irradiation. UVB irradiation at 50 mJ/cm^2 did not cause skin ulcers in either *MC5R*$^{-/-}$ or WT mice. UVB irradiation at 150 mJ/cm^2 caused skin ulcers in *MC5R*$^{-/-}$ but not in WT mice. UVB irradiation at 500 mJ/cm^2 caused skin ulcers in both WT and *MC5R*$^{-/-}$ mice (Figure 2a). Whereas ulcers occurred in all *MC5R*$^{-/-}$ mice 7 days after receiving 150 mJ/cm^2 of irradiation and occurred in all WT and *MC5R*$^{-/-}$ mice 7 days after receiving 500 mJ/cm^2 of irradiation (Figure 2b), the skin ulcers had healed in *MC5R*$^{-/-}$ mice 12 days after receiving 150 mJ/cm^2 of irradiation, but ulcers were still observed in WT and *MC5R*$^{-/-}$ mice 12 days after receiving 500 mJ/cm^2 of irradiation (Figure 2c). All *MC5R*$^{-/-}$ mice exposed to 150 mJ/cm^2 healed, whereas all those exposed to 500 mJ/cm^2 remained ulcerated (Figure 2d). The ulcer sizes were measured 7 days after irradiation to compare severity. At a dose of 150 mJ/cm^2, there were no skin ulcers in the WT mice. At a dose of 500 mJ/cm^2, there was no significant difference in skin damage between WT and *MC5R*$^{-/-}$ mice ($P < 0.01$) (Figure 2e). Transepidermal water loss (TEWL) was measured for examining the skin barrier function in *MC5R*$^{-/-}$ mice (Hattori et al., 2010). TEWL in *MC5R*$^{-/-}$ mice was revealed to be significantly higher than that in the WT mice before receiving 150 mJ/cm^2 of irradiation, indicating that the skin barrier function was originally disturbed in *MC5R*$^{-/-}$ mice before UVB irradiation ($P < 0.05$) (Figure 2f). Three days after receiving 150 mJ/cm^2 of irradiation, TEWL in *MC5R*$^{-/-}$ mice was kept at a high level similar to that before irradiation, whereas WT mice showed that TEWL increased to the same level as in *MC5R*$^{-/-}$ mice. Seven days after receiving 150 mJ/cm^2 of irradiation, TEWL decreased compared with that of 3 days after irradiation with no significant differences between *MC5R*$^{-/-}$ and WT mice (Figure 2f). Moreover, a dye exclusion assay was performed to evaluate the inverse skin permeability barrier function in neonates, and no remarkable differences were observed between *MC5R*$^{-/-}$ and WT mice (Figure 2g).

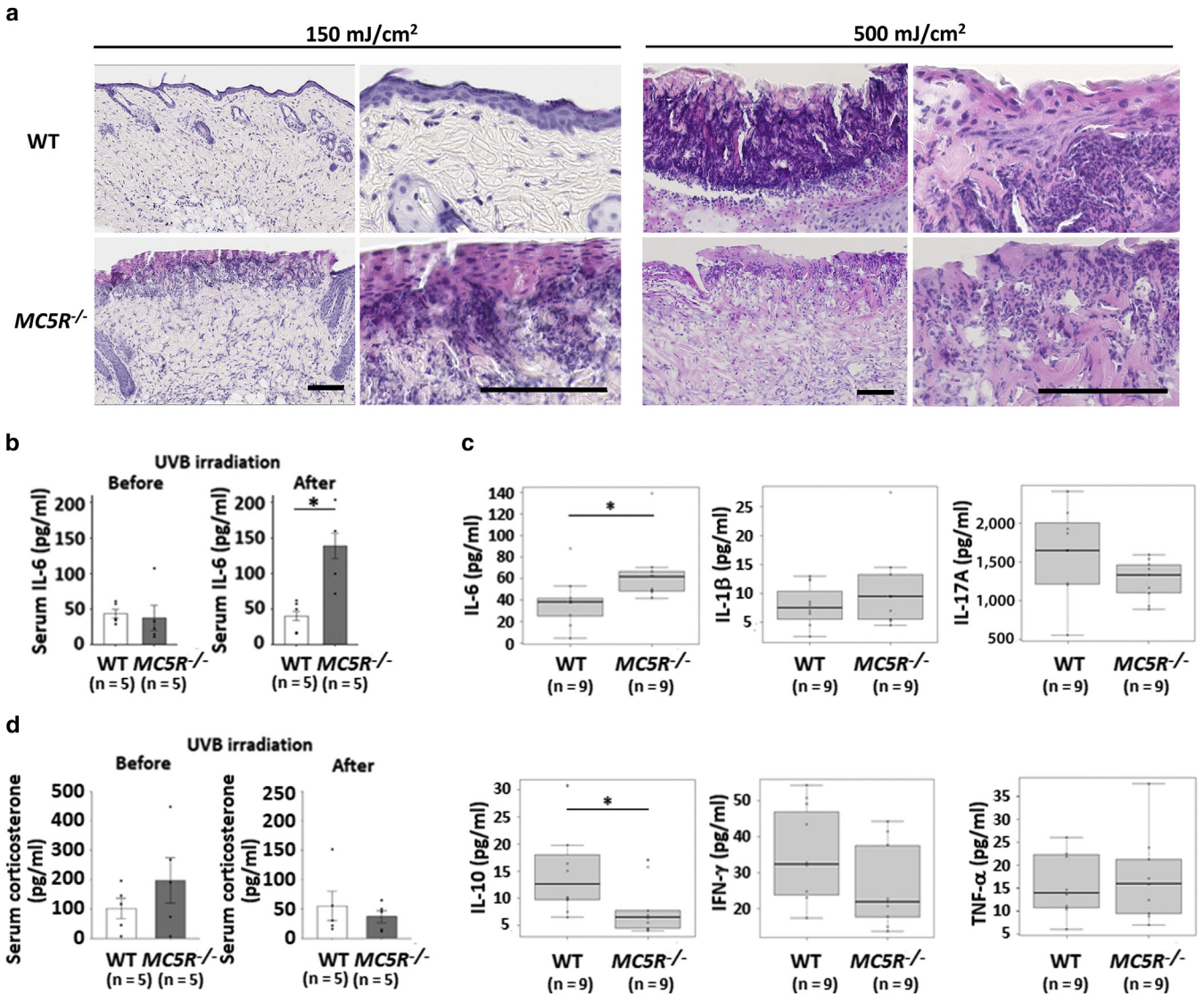

Figure 3. Changes in ulcerated skin tissues and inflammatory cytokines by UVB irradiation. (**a**) Histology of the ulcerated area 7 days after irradiation at 150 and 500 mJ/cm^2. Bar = 100 μm. (**b**) IL-6 was significantly elevated in *MC5R*$^{-/-}$ mice after irradiation. *$P < 0.05$. WT mice, $n = 5$; *MC5R*$^{-/-}$ mice, $n = 5$. (**c**) Multiplex T helper type 17 cytokine assay 7 days after irradiation at 150 mJ/cm^2. IL-6 was significantly higher, but IL-10 was lower in *MC5R*$^{-/-}$ than in WT mice. In other cytokines, there was no significant difference. *$P < 0.05$. WT mice, $n = 3$; *MC5R*$^{-/-}$ mice, $n = 3$. (**d**) Corticosterone showed no significant difference. Data are expressed as mean ± SEM. WT mice, $n = 5$; *MC5R*$^{-/-}$ mice, $n = 5$. WT, wild type.

Changes in ulcerated tissues and inflammatory cytokines by UVB irradiation

Seven days after irradiation of UVB at 150 mJ/cm^2, only slight acanthosis was observed in WT mice; however, *MC5R*$^{-/-}$ mice had crusting at the sites of epidermal defects and infiltration of inflammatory cells. Seven days after irradiation of UVB at 500 mJ/cm^2, skin ulcer lesions in WT mice showed eosinophilic thick crust containing partially remained epidermis and dermis with infiltration of several inflammatory cells, whereas in *MC5R*$^{-/-}$ mice, the dermis with inflammatory cell infiltration was covered with crust but defecting epidermis. In both groups, enlarged lymphatic vessels were observed (Figure 3a). Before UVB irradiation, the serum IL-6 levels were close to the detection limit in both WT and *MC5R*$^{-/-}$ mice. The serum IL-6 levels in WT mice remained close to the detection limit at 7 days after irradiation at 150 mJ/cm^2, whereas the serum IL-6 levels in *MC5R*$^{-/-}$ mice were significantly higher than those in WT mice ($P < 0.05$) (Figure 3b). The multiplex assay revealed that the IL-6 serum level was significantly higher and that the IL-10 serum level was significantly lower in *MC5R*$^{-/-}$ mice than in WT mice 7 days after UVB irradiation at 150 mJ/cm^2. The serum IL-1β, IL-17A, IFN-γ, and TNF-α levels did not differ between *MC5R*$^{-/-}$ and WT mice (Figure 3c). Regarding the serum corticosterone level, owing to the large variability in measurement values, no significant difference was found between *MC5R*$^{-/-}$ and WT mice both before and after UVB irradiation (Figure 3d).

Histological changes in nonulcerated areas after UVB irradiation

H&E-stained skin tissues of nonulcerated areas were compared before and on days 3, 7, and 12 after irradiation of

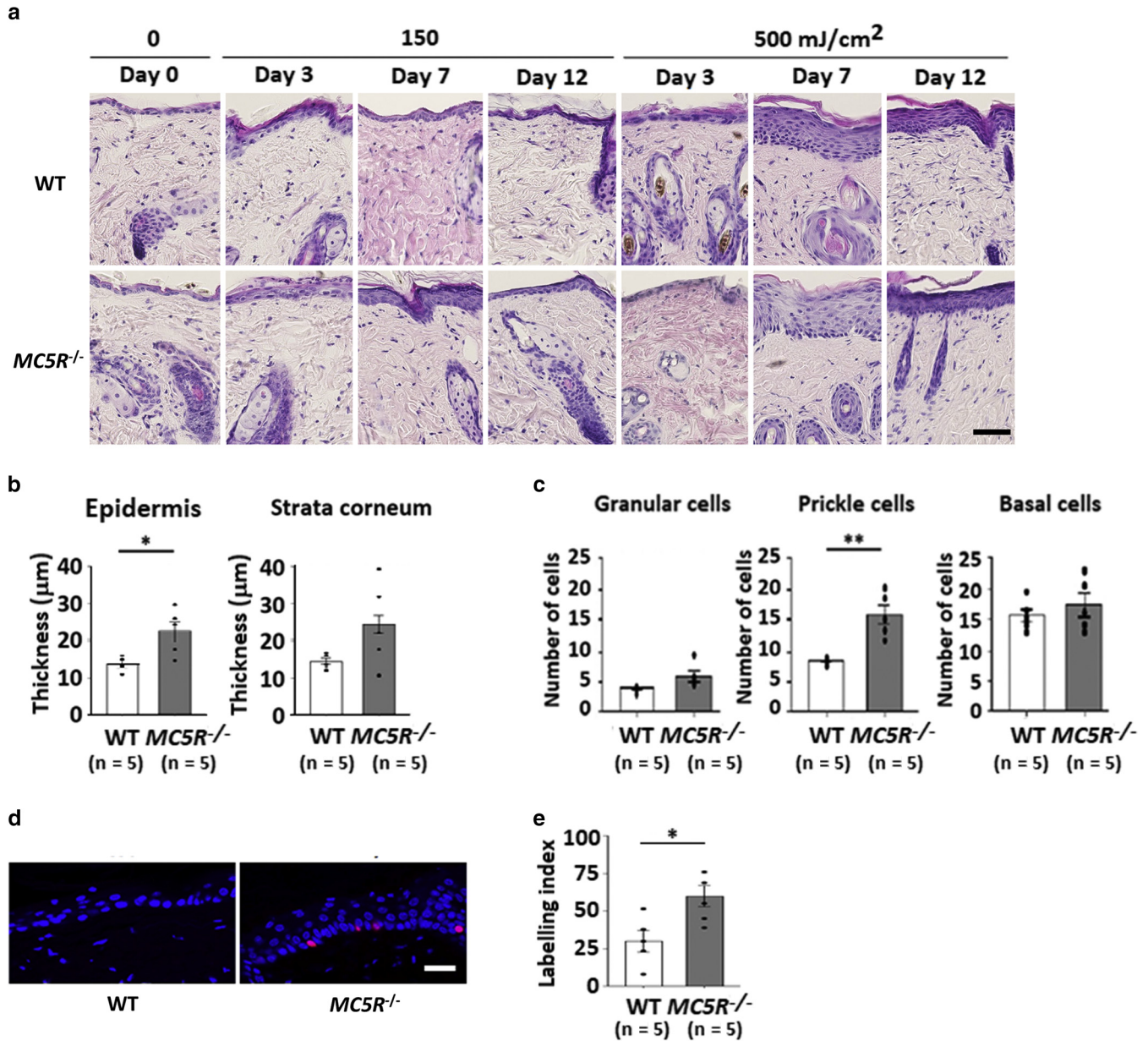

Figure 4. Chronological changes in the histological structure of the epidermis on nonulcer skin after irradiation. (**a**) The epidermis was thicker 7 days after irradiation in both WT and *MC5R*$^{-/-}$ mice. (**b, c**) Epidermal thickness and prickle cells were significantly increased in *MC5R*$^{-/-}$ compared with those in WT. No significant differences were found in the numbers of basal and granular cells. (**d, e**) The proliferating cells in the basal cell layer were detected with 5-ethynyl-2′-deoxyuridine after irradiation at 150 mJ/cm^2. *MC5R*$^{-/-}$ mice were significantly higher than WT mice. Data are expressed as mean ± SEM. *$P < 0.05$; **$P < 0.01$. WT mice, $n = 5$; *MC5R*$^{-/-}$ mice, $n = 5$. Bar = 50 μm. The nonulcerated area is not a healed ulcerated area. WT, wild type.

UVB at 150 mJ/cm^2. No remarkable differences were observed in the histology of the epidermis before UVB irradiation between WT and *MC5R*$^{-/-}$ mice. The epidermis thickened on the third day after UVB irradiation at 150 mJ/cm^2 in WT and *MC5R*$^{-/-}$ mice. Seven days after irradiation, WT mice showed a decreased thickness in the epidermis; conversely, *MC5R*$^{-/-}$ mice showed more pronounced thickening of the epidermis. At 12 days, the thickness of the epidermis in WT and *MC5R*$^{-/-}$ mice were decreased to the normal level, similar to that before irradiation. Seven days after UVB irradiation at 500 mJ/cm^2, the epidermises were drastically thickened in both WT and *MC5R*$^{-/-}$ mice. Twelve days after UVB irradiation, the epidermis tended to decrease in thickness in both groups but was thicker than that before UVB irradiation (Figure 4a). The total epidermis was significantly thicker in *MC5R*$^{-/-}$ than in WT mice ($P < 0.05$) (Figure 4b). The stratum corneum was not significantly different between the groups (Figure 4b). The prickle cell counts were significantly higher in *MC5R*$^{-/-}$ than in WT mice ($P < 0.01$) (Figure 4c), but there were no significant differences in the granule or basal cell counts. *MC5R*$^{-/-}$ mice were significantly higher on the 5-ethynyl-2′-deoxyuridine labeling index than WT on the seventh day after irradiation with 150 mJ/cm^2 of UVB irradiation, showing higher

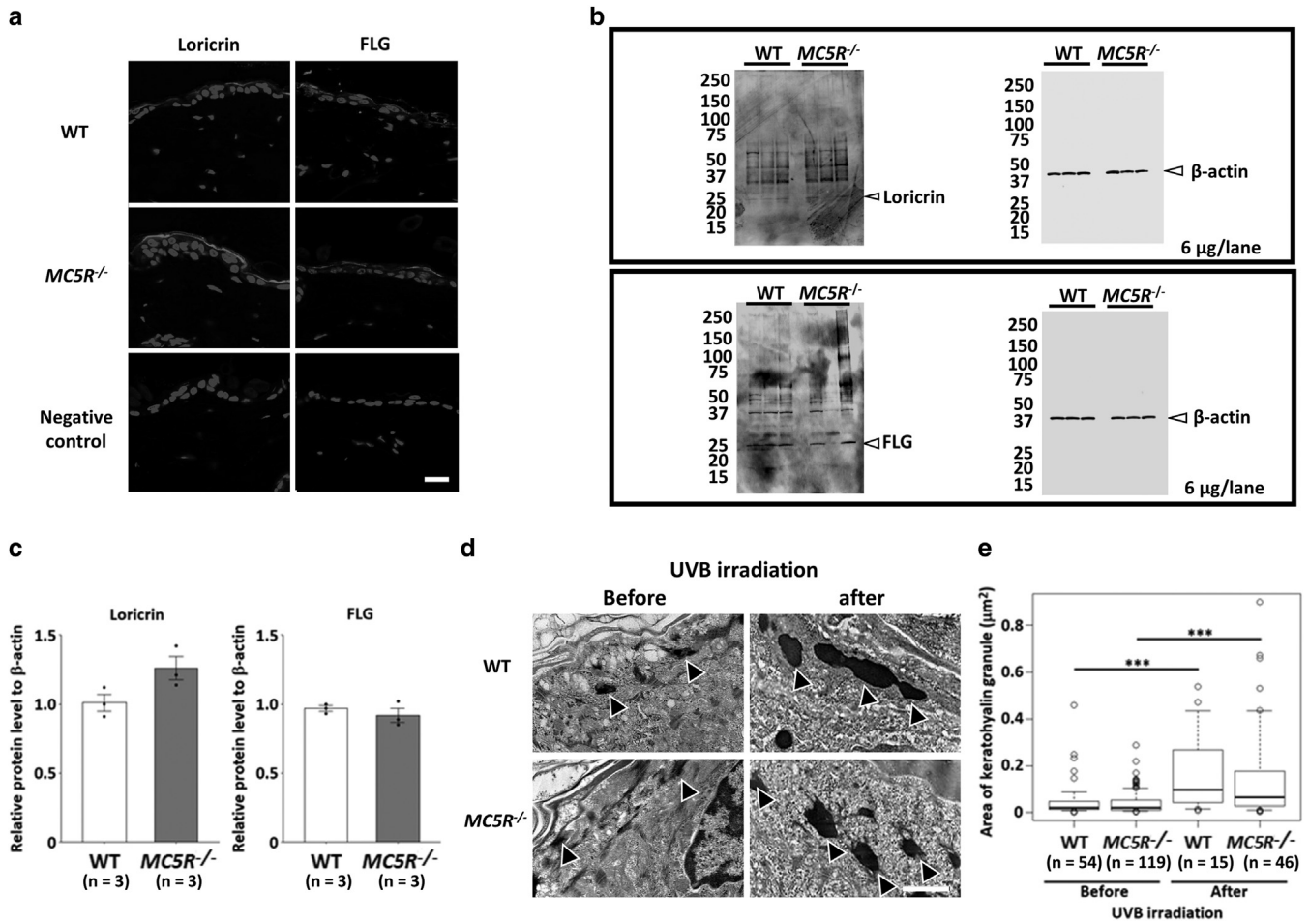

Figure 5. Histological analysis for skin barrier components. (**a**) Immunostaining showed loricrin and FLG in the surface layer of the epidermis in both WT and *MC5R*$^{-/-}$ mice before irradiation. Bar = 20 μm. (**b, c**) There were no significant differences in loricrin and FLG between WT and *MC5R*$^{-/-}$ mice in the skin before irradiation. WT mice, $n = 3$; *MC5R*$^{-/-}$ mice, $n = 3$. (**d, e**) The epidermis shows that keratohyalin granules (arrowhead) did not differ remarkably between WT and *MC5R*$^{-/-}$ mice before irradiation. After irradiation, keratohyalin granules were significantly increased in both WT and *MC5R*$^{-/-}$ mice. Data are presented as mean ± SEM. ***$P < 0.001$. WT mice, $n = 69$; *MC5R*$^{-/-}$ mice, $n = 165$. The nonulcerated area is not a healed ulcerated area. WT, wild type.

proliferative activity of KCs in *MC5R*$^{-/-}$ than in WT mice (Figure 4d and e).

Comparison of natural moisturizing factor and cornified envelope as skin barrier

In WT and *MC5R*$^{-/-}$ mice, loricrin and FLG were expressed near the granular layer (Figure 5a). There was no significant difference between the skins of WT and *MC5R*$^{-/-}$ mice before UVB irradiation (Figure 5b and c). The epidermis was observed using transmission electron microscopy (TEM). Pro-FLG–rich keratohyalin granules increased significantly in size after irradiation at 150 mJ/cm^2 in both WT and *MC5R*$^{-/-}$ mice. However, there were no significant differences between WT and *MC5R*$^{-/-}$ mice either before or after UVB irradiation (Figure 5d and e).

Comparison of intercellular lipids and lamellar granules

Next, we focused on lamellar granules (Odland bodies), which are important in skin barrier function as a corneocyte-bound lipid envelope against UVB. WT mice had many mature lamellar granules with bilayer membranes and lamellar structures, but the *MC5R*$^{-/-}$ mice had fewer lamellar granules with lamellar structures in the granular layer (stratum granulosum [SG] 1–2) and significantly more incomplete lamellar granules with moderate to translucent electron density (Figure 6a). The number of lamellar granules confirmed to have lamellar structures within the granular cells (SG1–2) was significantly lower in *MC5R*$^{-/-}$ than in WT mice both before and after UVB irradiation ($P < 0.05$) (Figure 6b). In the WT mice, the fusion secretion of lamellar granules was clearly observed between the stratum corneum and the SG (marginal zone), whereas fusion secretion was less visible in *MC5R*$^{-/-}$ mice (Figure 6c). The secretory area ratio in the marginal zone was significantly lower in *MC5R*$^{-/-}$ than in WT mice both before and after UVB irradiation ($P < 0.05$) (Figure 6d). An intercellular lipid accumulation between granular cells (SG1–3) was also more frequently observed in WT than in *MC5R*$^{-/-}$ mice (Figure 6e). The area of intercellular lipid accumulation between granular cells was significantly lower in *MC5R*$^{-/-}$ than in WT mice before and after UVB irradiation (before, $P < 0.01$; after, $P < 0.05$) (Figure 6f).

Seven days after UVB irradiation at 150 mJ/cm^2, electron microscopy of the nonulcerated skin tissue showed that the *trans*-Golgi network (TGN) containing immature lamellar

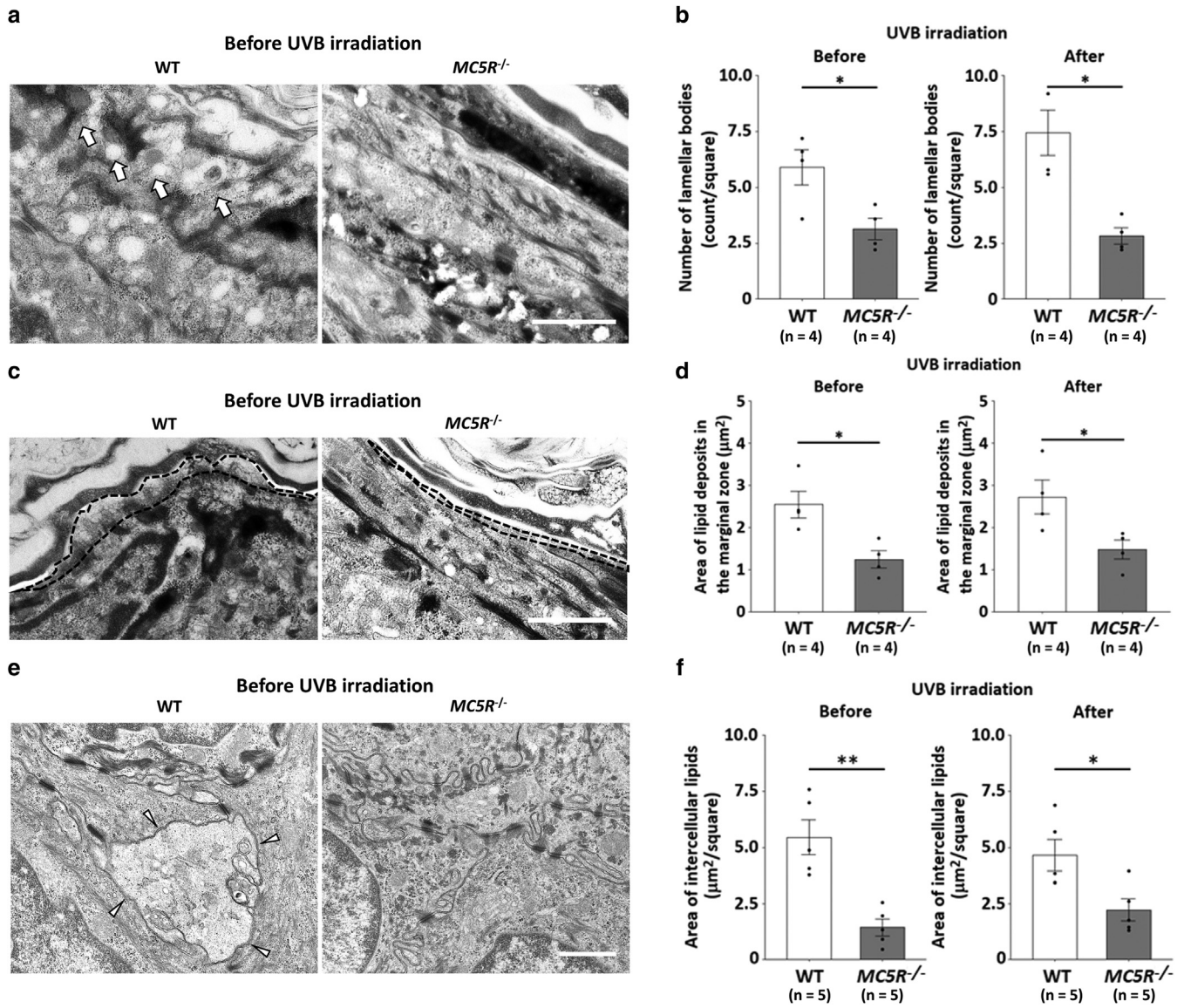

Figure 6. Intracellular dynamics of lamellar granules in the skin before and after irradiation in nonulcerated areas. (**a, b**) $MC5R^{-/-}$ mice had fewer matured lamellar granules (white arrows) than WT mice. (**c, d**) Lipid was discharged from lamellar granules to the marginal zone regularly (dotted line) in WT mice but rarely in $MC5R^{-/-}$ mice. $^{*}P < 0.05$. WT mice, $n = 4$; $MC5R^{-/-}$ mice, $n = 4$. Bar = 1 μm. (**e, f**) Accumulation of intercellular lipids between granular cells (white arrowheads) was significantly lesser in $MC5R^{-/-}$ than in WT mice. Data are presented as mean ± SEM. $^{*}P < 0.05$; $^{**}P < 0.01$. WT mice, $n = 5$; $MC5R^{-/-}$ mice, $n = 5$. Bar = 1 μm. The nonulcerated area is not a healed ulcerated area. WT, wild type.

granules was expanded in $MC5R^{-/-}$ but not in WT mice, and WT mice showed numerous independent mature lamellar granules (Figure 7a). Using qPCR to examine the skin tissue before UVB irradiation, the expressions of *Abca12*, which is involved in the transport of lipids into lamellar granules, and *Fatp4*, which is required for the synthesis of acyl glucosylceramides, were compared. No significant differences in the expressions of these genes between WT and $MC5R^{-/-}$ mice were observed (Figure 7b). Thin-layer chromatography (TLC) analysis on ceramides in the epidermis showed that ceramide was determined in both $MC5R^{-/-}$ and WT mice with no remarkable difference (Figure 7c). This result was supported by the semiquantitative densitometric analysis of ceramide spots with ImageJ (National Institutes of Health, Bethesda, MD), revealing no significant difference in the quantities of ceramide between $MC5R^{-/-}$ and WT mice. This analysis of the ceramide in the epidermis with TLC showed that differences in ceramide components, including various ceramides, between $MC5R^{-/-}$ and WT mice were not clearly defined in the epidermis (Figure 7c and d).

DISCUSSION

In this study, we found that lower doses of UVB irradiation caused more skin ulcers and excessive inflammatory conditions in $MC5R^{-/-}$ than in WT mice because as we investigated the role of MC5R in skin injuries caused by UVB irradiation in mice. An irradiation dose of 150 mJ/cm^2 of UVB in a mouse is the equivalent of an irradiation dose that would cause erythema in a healthy person (Gambichler et al., 2006). Examining each cell layer of the epidermis, we found

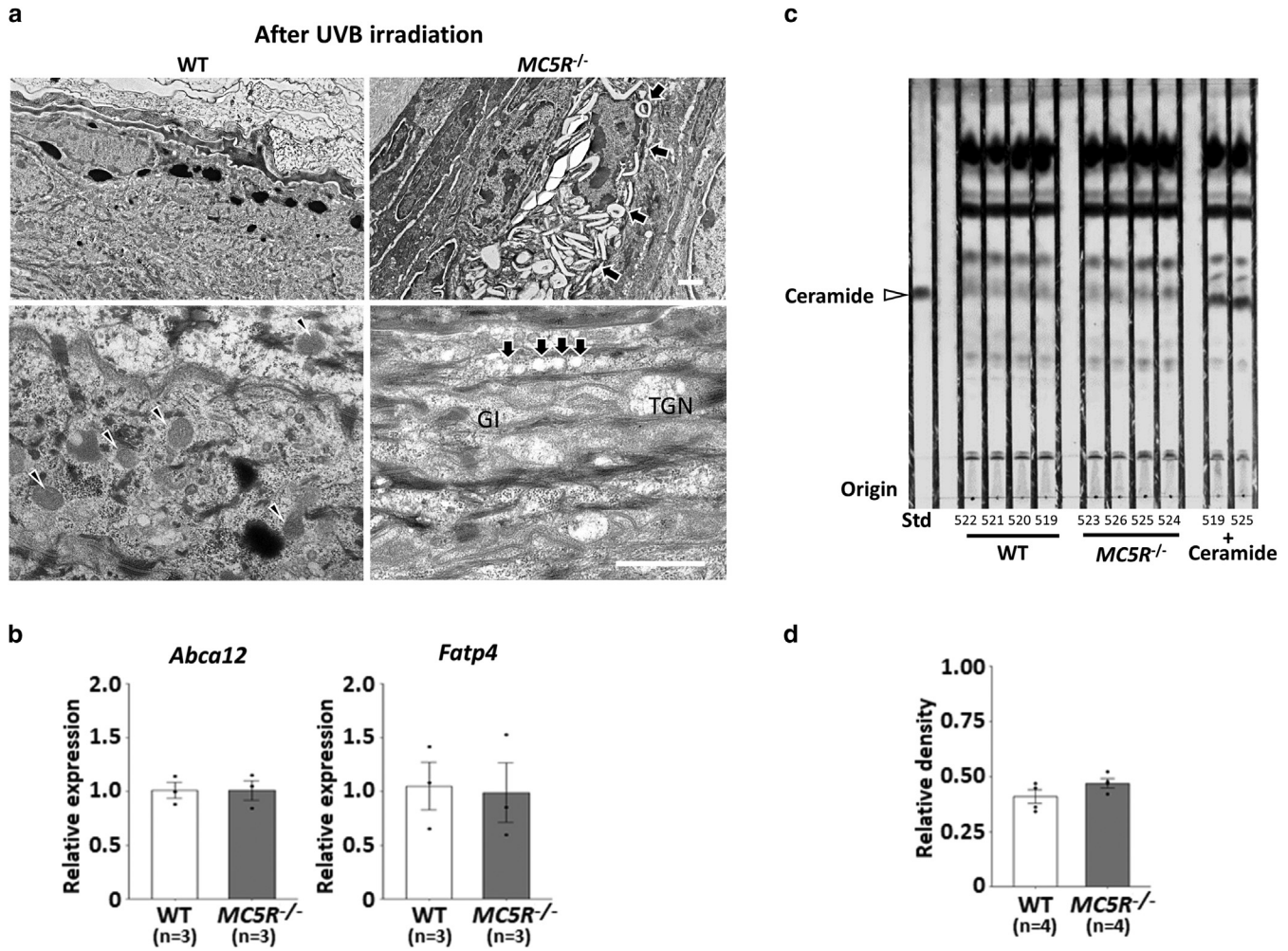

Figure 7. Comparison of lipid synthesis and transport. (**a**) After irradiation, $MC5R^{-/-}$ mice showed an expanded TGN (arrows). WT mice showed numerous mature lamellar granules (arrowheads). (**b**) *Abca12* and *Fatp4* expression in the skin before irradiation between $MC5R^{-/-}$ and WT mice. Data are expressed in mean ± SEM. $*P < 0.05$; $**P < 0.01$. WT mice, $n = 3$; $MC5R^{-/-}$ mice, $n = 3$. Bar = 1 μm. (**c, d**) Analysis of ceramides in the epidermis with thin-layer chromatography. Differences in ceramide components between $MC5R^{-/-}$ and WT mice were not clearly defined (WT mice: 519; $MC5R^{-/-}$ mice: 525). WT mice, $n = 4$; $MC5R^{-/-}$ mice, $n = 4$. The nonulcerated area is not a healed ulcerated area. +Ceramide denotes the extracted lipid samples with Std; GI indicates the Golgi cistern. Std, standard ceramide; TGN, *trans*-Golgi network; WT, wild type.

that the response of KCs to UVB irradiation–induced inflammation, such as the thickening of the epidermis, which was supported by increased proliferative activity in basal cells, was not disturbed in $MC5R^{-/-}$ mice.

The functional assay was performed to evaluate the skin barrier, revealing that TEWL was approximately 10 times higher in $MC5R^{-/-}$ than in WT mice before UVB irradiation. Three days after UVB irradiation, $MC5R^{-/-}$ mice kept TEWL at a high level, and WT mice showed an increase of TEWL to the same level as that in $MC5R^{-/-}$ mice. Seven days after UVB irradiation, TEWL in both groups was decreased to the normal level. These findings indicated that the skin barrier function in $MC5R^{-/-}$ mice was already impaired at the time of UVB exposure, resulting in more severe damage even with mild UVB irradiation in $MC5R^{-/-}$ mice. Interestingly, when comparing the TEWL value in $MC5R^{-/-}$ mice before UVB irradiation and 7 days after irradiation, it was revealed that UVB exposure could improve the skin barrier function in $MC5R^{-/-}$ mice, which was supported by an increase in the thickness and proliferation of basal cells in the epidermis after UVB irradiation, as shown in Figure 4. In neonates, dye exclusion assay showed no obvious defects in $MC5R^{-/-}$ mice, although TEWL and body weight loss assays were not performed.

Mutations to the epidermal barrier function, including deficiencies in KLF4 (Segre et al., 1999), claudin 1 (Furuse et al., 2002), and FATP4 (Herrmann et al., 2003; Yamamoto et al., 2020), have been reported to be lethal in neonates. KLF4-deficient neonates suffer a loss of the epidermal barrier that includes the cornified envelope, a scaffold for lipid organization with a 20-fold increase in TEWL (Segre et al., 1999). Mice deficient in claudin 1 lack a tight junction barrier function in the strata corneum and granulosum (Furuse et al., 2002). FATP4-deficient neonates exhibit a severe barrier function impairment owing to a defect in barrier lipid ω-O-acylceramide synthesis (Herrmann et al., 2003; Yamamoto et al., 2020). Thus, such mutations to the skin barrier function result in very severe phenotypes. When we compare

MC5R$^{-/-}$ mice, which can have long lives without remarkable phenotypes if they are not exposed to UVB, with mice suffering from the mutations mentioned earlier, the impairment to the barrier function in *MC5R*$^{-/-}$ mice seems moderate. Further studies to elucidate the underlying mechanisms that affect the skin barrier function in *MC5R*$^{-/-}$ mice, including more detailed functional assays in neonates and in vitro assays using three-dimensional cultures of reconstructed epidermises, are needed.

The skin barrier is composed of sebum membranes secreted by sebaceous glands; cornified envelope, including corneocyte-bound lipid envelope; and natural moisturizing factor (Bouwstra and Ponec, 2006; Elias, 2012; Ponec et al., 2000). In this study, although the sebaceous membranes formed in the epidermal surface layer in *MC5R*$^{-/-}$ mice showed no significant difference between *MC5R*$^{-/-}$ and WT mice, sebaceous gland hypoplasia was observed in *MC5R*$^{-/-}$ mice, supporting the findings of previous reports (Eisinger et al., 2011; Zhang et al., 2006). Although involucrin and FLG play important roles in cornified envelope formation, their expression did not differ between WT and *MC5R*$^{-/-}$ mice before UVB irradiation. Next, the production of lamellar granules and their secretion in the marginal and intercellular zones were examined, which are the major components of the corneocyte-bound lipid envelope, which is the second step of cornified envelope formation (Candi et al., 2005, 2016; Reynier et al., 2016). The ceramide secreted from the lamellar granules forms lamellar structures with fatty acids and cholesterol that create skin barriers against UVB exposure (Imokawa, 2014; Oda et al., 2010). In this study, TLC analysis showed that ceramide was contained in the epidermis in *MC5R*$^{-/-}$ mice at the same level as that in WT mice. Unfortunately, the difference of ceramides species in the epidermis between *MC5R*$^{-/-}$ and WT mice was not characterized using TLC assay. A more sensitive approach, including liquid chromatography with tandem mass spectrometry, is needed to elucidate this issue.

However, morphological analysis with TEM provided the critical findings associated with the skin barrier function. The number of normal lamellar granules was decreased in *MC5R*$^{-/-}$ mice; conversely, the number of granules with incomplete lamination increased. TEM study also revealed decreased secretion into the marginal zone in *MC5R*$^{-/-}$ mice. The expression of *Fatp4* (Yamamoto et al., 2020) for the synthesis of acyl glucosylceramides and *Abca12* (Crumrine et al., 2019; Wertz, 2018) for lipid transport containing acyl glucosylceramides into lamellar granules in the epidermis without UVB irradiation did not differ between WT and *MC5R*$^{-/-}$ mice, suggesting that ceramide synthesis and lipid transport into TGN were not affected in *MC5R*$^{-/-}$ mice. Suggesting impaired separation of lamellar granules from the TGN resulting in the accumulation of lamellar granules to expand the TGN in *MC5R*$^{-/-}$ mice, extensively expanded TGNs that stored a large quantity of lamella-like lipid aggregations were observed in the granular layer of *MC5R*$^{-/-}$ mice.

Abnormal accumulation of lipids in the TGN and endosome and/or activation of the inflammatory system may cause endoplasmic reticulum stress, thus inducing cell death, which could initially trigger skin ulcers. This study supports previous reports that ceramide, whose production is enhanced by irradiation of UVB or intracellular oxidative stress, induces apoptosis (Uchida et al., 2010, 2003).

The skin hypothalamic–pituitary–adrenal axis, an antistress hormone network that inhibits inflammatory responses, possibly did not work well in *MC5R*$^{-/-}$ mice. Generally, MC2R is mainly responsible for the inflammatory regulatory system of the hypothalamic–pituitary–adrenal axis (Jozic et al., 2015; Skobowiat et al., 2011). Together with MC2R, MC5R localizes in the KC and the zona fasciculata of the adrenal cortex secreting glucocorticoids, but its function is not clear (Dores, 2016). To examine the response of inflammatory stress through the skin hypothalamic–pituitary–adrenal axis, peripheral blood corticosterone was determined quantitatively. However, owing to the possibly large effect of circadian variation, no clear difference was detected between WT and *MC5R*$^{-/-}$ mice after UVB irradiation (Figure 3d). A more elegant assay system is needed to reveal the involvement of MC5R in stress response. Recently, the immunomodulatory mechanism of melanocortin receptors has gained attention. As an inflammatory control by a completely different pathway from the hypothalamic–pituitary–adrenal axis, MC5R was reported to regulate T-cell induction into autoantigen-responsive FOXP3^{+}CD4^{+} regulatory T cells (Clemson et al., 2017; Lee and Taylor, 2013; Lee et al., 2016; Muhammad et al., 2019). IL-10 induced by FOXP3^{+}CD4^{+} regulatory T cell is known to be associated with immune response suppression in the skin (O'Garra et al., 2004). In this study, impairment of IL-10 induction was revealed using a multiplex assay in *MC5R*$^{-/-}$ mice after UVB irradiation. It is suggested that MC5R-dependent induction of FOXP3^{+}CD4^{+} regulatory T cell is impaired in *MC5R*$^{-/-}$ mice, resulting in the increased severity of UV-induced skin injury. To elucidate the detailed mechanism regarding the immunological aspect, a further functional study is required.

In conclusion, this study revealed that MC5R$^{-/-}$ mice exhibit increased sensitivity to UVB irradiation resulting in increased serum IL-6 levels and infiltration of inflammatory cells and that MC5R$^{-/-}$ mice are associated with reduced lamellar granules and reduced lipid secretion from the epidermis, which are possibly associated with the impairment of skin barrier function.

Finally, it is interesting that the melanocortin receptor species of MC1R, MC2R, and MC5R cleverly divide their roles to contribute to the maintenance of skin homeostasis, bearing in mind that it was clarified that MC1R is involved in the skin defense mechanism by the melanin pigment induction, that MC2R is involved in the anti-inflammation response by the glucocorticoid secretion, and finally that MC5R is involved in the sensitivity and barrier function to UVB irradiation.

MATERIALS AND METHODS

Mice

The sperm of *MC5R*$^{-/-}$ mice was purchased from Jackson Laboratory (Chen et al., 1997), and eggs from female mice of C57BL/6J (Japan SLC, Shizuoka, Japan) were fertilized in vitro to reconstitute the strain of *MC5R*$^{-/-}$ mice. Male *MC5R*$^{-/-}$ and WT mice (aged 8–35 weeks) were used for further study. They were housed in a

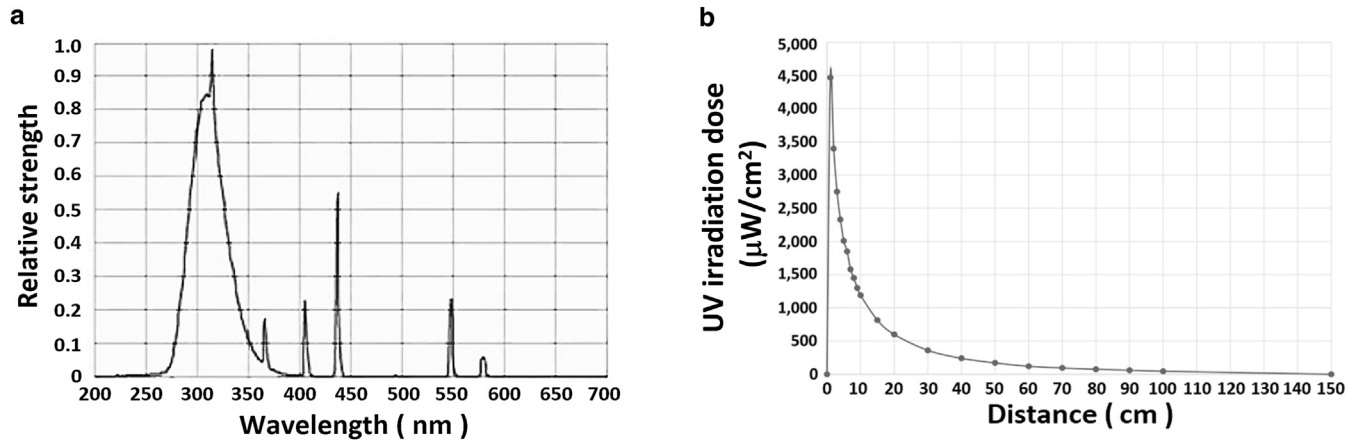

Figure 8. UVB lamp information. Source: Sankyo Electric (Osaka, Japan).

room with controlled temperature (21−23 °C), humidity (45−65%), and light (7:00 AM to 7:00 PM). Food and water were freely available ad libitum. To minimize suffering, the mice were anesthetized by an intraperitoneal injection of a mixture of medetomidine (0.3 mg/kg body weight), midazolam (4 mg/kg body weight), and butorphanol (5 mg/kg body weight). All procedures involved in this study were performed in strict accordance with the guidelines for the Care and Use of Laboratory Animals of Kanazawa Medical University (Uchinada, Japan). The protocol was approved by the Ethics Committee on Animal Experiments and DNA Recombination Experiments of the Kanazawa Medical University (permit numbers: 2020-52 and 2019-4).

UVB irradiation

A UVB lamp (range, 280−350 nm; peak, 306 nm; see Figure 8 for details; GL20SE 20 W, Sankyo Electronics, Fukuoka, Japan) was used for irradiation. Mice were shaved with clippers under anesthesia and were laid on their left sides. The capacity of UV rays was determined by multiplying the value measured with a dosimeter (260−320 nm, X1 Optometer, Gigahertz-Optik, Movelier, Switzerland) by the exposure time. The dose of UVB irradiation was time controlled, and experiments were conducted at 50, 150, and 500 mJ/cm^2.

Light microscopy

For light microscopy, mice were first anesthetized as described earlier. The preirradiated skin fragments were taken from the center of the right side of the chest of each mouse. The postirradiated skin was collected from the center of the left side of the chest. When ulcers appeared, the ulcer lesion and three different sites >5 mm away from the ulcer were collected as nonulcer areas 3, 7, and 12 days after UVB irradiation. Specimens were fixed in phosphate-buffered (50 mM; pH 7.4) 4% paraformaldehyde (WAKO, Osaka, Japan) at 4 °C overnight. Paraffin sections of 8 μm for H&E staining and of 5 μm for immunostaining were cut.

The total thickness of the epidermis and the thickness of each layer within the epidermis stained with H&E were measured on an image taken with a Nanozomer (Hamamatsu Photonics, Hamamatsu, Japan). Measurements were made at three locations every 100 μm along the epidermal surface in each section, and a total of nine measurements per individual were averaged. The number and size of sebum cells per section were measured in a 1-mm wide vertical column set on the images captured using Nanozomer (Hamamatsu Photonics), and the mean value of measurements was calculated from three regions per slide. The cell size (area) was also measured in the cells with nuclei.

Frozen skin was cut into 10-μm-thick sections, washed in 50% ethanol, and incubated in Sudan III (Chroma-Gesellschaft Schmid GmbH, Kongen, Germany) solution saturated with 70% ethanol. After the second wash in 50% ethanol, these sections were counterstained with Mayer's hematoxylin (Vector Laboratories, Burlingame, CA). Sections were then colored with diluted lithium carbonate and observed under the light microscope.

TEM

The samples were dehydrated in ethanol and finally embedded in LR White (medium grade; London Resin, Berkshire, England). Ultrathin sections of 100 nm were cut using the PT-X Power Tome ultramicrotome (Boeckeler Instruments, Tucson, AZ) and counterstained with uranyl acetate and lead citrate. They were then observed using the JEM-1400 Plus transmission electron microscope (JEOL, Tokyo, Japan) at an accelerating voltage of 80 kV, with images captured at the frame size of 3,296 × 2,472 pixels.

The TEM images of SG1–2 were magnified at 10,000 in each group and were serially stacked using ImageJ software, after which five images were randomly picked through a lottery and were used in blinded quantitative imaging analyses. The ratio of the area of secretion between the stratum corneum and SG1 was measured in a whole-captured frame. The number of lamellar granules in SG1–2 was measured within 20 μm^2 on the TEM images (Reynier et al., 2016). We measured the areas of 69 lamellar granules in WT and 165 lamellar granules in *MC5R*$^{-/-}$ mice.

Immunostaining

To activate them, antigens were heated at 95 °C in a 10 mM citric acid solution or 10 mM citrate buffer (pH: 6.0). After blocking with 1% BSA in Tris-buffered saline or Mouse-on-Mouse Kit (Vector Laboratories), the sections were incubated overnight at 4 °C with goat anti-MC5R mAb (1:500; Abcam, Cambridge, United Kingdom), rabbit anti-FLG polyclonal antibody (1:500; Gene Tex, Irvine, CA), rabbit anti-loricrin polyclonal antibody (1:1,000; Abcam), or mouse anti-involucrin mAb (1:200; Invitrogen, Carlsbad, CA). The sections were incubated for 30 minutes in a solution of 0.3% hydrogen peroxide in methanol to block endogenous peroxidase, were then incubated for 1 hour with secondary antibodies (ImmPRESS-HRP Anti-Goat IgG Polymer Detection Kit, Vector Laboratories), and were visualized using the liquid diaminobenzidine substrate chromogen

system (Dako, Santa Clara, CA) for 3–5 minutes. Secondary antibodies (1:500; Alexa Fluor 594–labeled donkey antirabbit IgG, Invitrogen) or Alexa Fluor 594–labeled donkey anti-mouse IgG (1:500; Invitrogen) were used. Sections were counterstained with hematoxylin for light microscopy or with Hoechst 33342 (Invitrogen) for confocal laser scanning microscopy (LSM710, Zeiss, Oberkochen, Germany). For negative controls, species-matched normal IgG was used at the same concentration.

Evaluation of skin barrier function

TEWL was measured using a VAPO SCAN (AS-VT 100RS, Asahi Biomed, Yokohama, Japan). After shaving, TEWL measurement was triplicated at four sites on the left forefoot base, thorax, abdomen, and hindfoot base. The time points for measurement were before UVB irradiation and after UVB irradiation at 150 mJ/cm^2 at 3 and 7 days (Yamamoto et al., 2020). To evaluate the inverse skin permeability, a dye exclusion assay was performed. Pups on the day of delivery were used to evaluate the inverse skin permeability barrier function. Newborn pups (*MC5R*$^{-/-}$: n = 2, WT: n = 4) after euthanasia on the day of delivery were incubated in methanol for 5 minutes, washed in PBS, and then immersed in 0.1% (wt/vol) toluidine blue in PBS solution at 4 °C for 2 hours.

5-Ethynyl-2′-deoxyuridine proliferation assay

Cell proliferation was detected with 5-ethynyl-2′-deoxyuridine using the 5-ethynyl-2′-deoxyuridine Cell Proliferation Assay Kit (Ribobio, Guangzhou, China). The cell nuclei were counterstained with Hoechst 33342 and were observed with LSM710 (Zeiss). Using five random fields per section, a positive-to-negative ratio of 5-ethynyl-2′-deoxyuridine was calculated. Four sections were used in each group.

ELISA

While the mice were under anesthesia, the serum was collected from the heart and stored at −80 °C until use. The serum IL-6 level was measured by ELISA using a Mouse IL-6 ELISA MAX (Biolegend, San Diego, CA), according to the manufacturer's instructions. Measurements were triplicated by 2104 EnVision (PerkinElmer, Waltham, MA). Five mice were used in each group. The serum total corticosterone levels were measured using a Corticosterone ELISA Kit (Enzo Biochem, Farmingdale, NY) according to the manufacturer's instructions (www.enzolifesciences.com).

Multiplex cytokine bead array assay

On day 7 after UVB irradiation at 150 mJ/cm^2, the serum IL-6, IL-1β, IL10, IL-17A, IFN-γ, and TNF-α levels in WT (n = 9) and *MC5R*$^{-/-}$ (n = 9) mice were measured using the Bio-Plex Pro Mouse Cytokine T helper type 17 Panel by multiplex cytokine bead array assay (Bio-rad Laboratories, Hercules, CA) according to the manufacturer's instructions. Each sample was measured in duplicate using the Bio-Plex MAGPIX system (Bio-Rad Laboratories).

Western blot analysis

PRO-PREP protein extract (iNtRON Biotechnology, Kirkland, WA) was used to purify the skin tissues according to the manufacturer's instructions. The protein contents were measured using a DS-11 Spectrophotometer (DeNovix, Wilmington, DE), denatured in a sample buffer containing 10% mercaptoethanol for 5 minutes at 100 °C, separated by SDS-PAGE, and transferred to a SuperSep Ace membrane (WAKO). After blocking with 1% BSA, the membranes were incubated overnight at 4 °C with anti-FLG polyclonal antibody (1:500; Gene Tex), anti-loricrin polyclonal antibody (1:1,000; Abcam), or anti-involucrin mAb (1:200; Invitrogen). β-Actin (1:1,000; Santa Cruz Biotechnology, Santa Cruz, CA) was used as a loading control. The membranes were incubated at room temperature with either the goat antirabbit IgG heavy and light chains (1:3,000; Abcam) or mouse true blot (1:1,000; Cambrex BioScience Rockland, Rockland, ME) secondary antibody. The signals were detected using a Super Signal West Pico PLUS (Thermo Fisher Scientific, Waltham, MA). For reblotting, Restore Plus Western Blot Stripping Buffer (Thermo Fisher Scientific) was used to strip the membranes. ImageJ software was used to quantify the band intensities on each membrane.

qPCR

The total RNA of the skin was extracted using ISOGENII (Nippon Gene, Tokyo, Japan). cDNA was synthesized from 2.5 μg of RNA using SuperScript III reverse transcriptase (Invitrogen). qPCR was performed using cDNA with GeneAce SYBR qPCR Mix a No ROX (Nippon Gene). Using the $2^{-\Delta\Delta Ct}$ method, expressions of *Abca12* and *Fatp4* were normalized to the housekeeping genes' 18S ribosomal RNA (Applied Biosystems, Bedford, MA). Reactions were performed in triplicate. PCRs were carried out for 45 cycles under annealing at 95 °C for 30 seconds and under extension at 60 °C for 1 minute. The primer sequences for *Abca12* were 5′-AAGATGCTGACTGGAGACATAATTC-3′ (forward) and 5′-GAAATACAAGTGCTCTTCCACAGTT-3′ (reverse) and those for *Fatp4* were 5′-GCCCTGGACCCAGGTGGGATTCTCC-3′ (forward) and 5′-GAGTACTCATCCAGCTGGCGGAAGG-3′ (reverse).

Lipid extraction and TLC analysis

The whole skin from the auricle was collected (n = 4 in *MC5R*$^{-/-}$ and WT mice) and immersed in 1 M sodium chloride at 4 °C for 9 days (Scaletta et al., 1978). Then, the epidermis was carefully detached from the dermis and was used for further lipid analysis. Lipids were extracted from the epidermal sheets using a mixture of chloroform, methanol, and water at room temperature overnight using Bligh and Dyer method (Bligh and Dyer, 1959). Lipid extracts from 50 mg of epidermis were dissolved in 90 μl of chloroform, and 5 μl per mice were subjected to TLC analysis. In TLC analysis using silica gel 60, the solvent system was chloroform/methanol/acetic acid (95:5:0.1 vol/vol/vol). Lipids were detected by spraying 5% sulfuric acid vol/vol onto TLC plates and heating at 180 °C for 15 minutes. Ceramide in the collected epidermis was identified by loading C16 ceramide (N-Hexadecanoyl-D-erythro-sphingosine, Matreya, State College, PA) as the standard, and densitometric analysis was performed to semiquantitatively compare the ceramide contents between *MC5R*$^{-/-}$ and WT mice with densitometric analysis using ImageJ (Rasband, 1997–2012).

Statistical analysis

One-way ANOVA and Tukey's posthoc test or the Mann–Whitney *U* test was performed to determine the differences between the mean values of measurement using the program R, with values considered significant at $P < 0.05$.

Data availability statement

Datasets related to this article can be found at https://doi.org/10.17632/pzrd6kvs99.1, hosted at Mendeley Data (Hatta, Toshihisa [2021], Role of Melanocortin 5R in Epidermis, Mendeley Data, V1, https://doi.org/10.17632/pzrd6kvs99.1).

ORCIDs
Akari Shintani: https://orcid.org/0000-0001-7298-9127
Hiromi Sakata-Haga: https://orcid.org/0000-0002-4928-0301
Keiichi Moriguchi: https://orcid.org/0000-0003-4131-5626

Mitsuhiro Tomosugi: https://orcid.org/0000-0002-0635-9415
Daisuke Sakai: https://orcid.org/0000-0001-5538-4927
Tsuyoshi Tsukada: https://orcid.org/0000-0003-4404-0103
Makoto Taniguchi: https://orcid.org/0000-0001-5920-8285
Masahide Asano: https://orcid.org/0000-0002-9087-6481
Hiroki Shimada: https://orcid.org/0000-0003-1774-5327
Hiroki Otani: https://orcid.org/0000-0002-0331-3008
Hiroki Shoji: https://orcid.org/0000-0002-4863-389X
Junko Hatta: https://orcid.org/0000-0001-7082-4038
Takashi Mochizuki: https://orcid.org/0000-0002-3793-980X
Toshihisa Hatta: https://orcid.org/0000-0001-7992-2793

AUTHOR CONTRIBUTIONS

Conceptualization: TH; Data Curation: AS, JH; Formal Analysis: TT, HSH, KM, HS, MTo, MTa; Funding Acquisition: TH; Investigation: AS, JH, DS; Methodology: TH; Project Administration: TH; Resources: TH; Software: TH; Supervision: TH; Validation: HS; Visualization: AS; Writing - Original Draft Preparation: AS; Writing - Review and Editing: HO, TM, TH

ACKNOWLEDGMENTS

The authors thank Masami Kojima for technical advice in UVB irradiation, Tomoko Yasuda for her help in histological preparation, Mayumi Mitani for technical support, and Yuko Imaoka and Tsunao Yoneyama for technical support with the transmission electron microscopy analysis. This work was supported by the Japan Society for the Promotion of Science KAKENHI (grant numbers 15K09713, 16H05364, and 18K11659). The authors thank Sankyo Electric for providing the UVB lamp information and Enago (www.enago.jp) for the English language review.

CONFLICT OF INTEREST

The authors state no conflict of interest.

REFERENCES

Bligh EG, Dyer WJ. A rapid method of total lipid extraction and purification. Can J Biochem Physiol 1959;37:911–7.

Bouwstra JA, Ponec M. The skin barrier in healthy and diseased state. Biochim Biophys Acta 2006;1758:2080–95.

Candi E, Knight RA, Panatta E, Smirnov A, Melino G. Cornification of the skin: a non-apoptotic cell death mechanism. eLS. Hoboken, NJ: John Wiley & Sons, Ltd; 2016. p. 1–10.

Candi E, Schmidt R, Melino G. The cornified envelope: a model of cell death in the skin. Nat Rev Mol Cell Biol 2005;6:328–40.

Catania A, Gatti S, Colombo G, Lipton JM. Targeting melanocortin receptors as a novel strategy to control inflammation. Pharmacol Rev 2004;56:1–29.

Chen W, Kelly MA, Opitz-Araya X, Thomas RE, Low MJ, Cone RD. Exocrine gland dysfunction in MC5-R-deficient mice: evidence for coordinated regulation of exocrine gland function by melanocortin peptides. Cell 1997;91:789–98.

Clemson CM, Yost J, Taylor AW. The role of alpha-MSH as a modulator of ocular immunobiology exemplifies mechanistic differences between melanocortins and steroids. Ocul Immunol Inflammm 2017;25:179–89.

Cone RD. Studies on the physiological functions of the melanocortin system. Endocr Rev 2006;27:736–49.

Crumrine D, Khnykin D, Krieg P, Man MQ, Celli A, Mauro TM, et al. Mutations in recessive congenital ichthyoses illuminate the origin and functions of the corneocyte lipid envelope. J Invest Dermatol 2019;139:760–8.

Dores RM. Hypothesis and theory: revisiting views on the co-evolution of the melanocortin receptors and the accessory proteins, MRAP1 and MRAP2. Front Endocrinol (Lausanne) 2016;7:79.

Eisinger M, Li WH, Anthonavage M, Pappas A, Zhang L, Rossetti D, et al. A melanocortin receptor 1 and 5 antagonist inhibits sebaceous gland differentiation and the production of sebum-specific lipids. J Dermatol Sci 2011;63:23–32.

Elias PM. Structure and function of the stratum corneum extracellular matrix. J Invest Dermatol 2012;132:2131–3.

Furuse M, Hata M, Furuse K, Yoshida Y, Haratake A, Sugitani Y, et al. Claudin-based tight junctions are crucial for the mammalian epidermal barrier: a lesson from claudin-1-deficient mice. J Cell Biol 2002;156:1099–111.

Gambichler T, Moussa G, Tomi NS, Paech V, Altmeyer P, Kreuter A. Reference limits for erythema-effective UV doses. Photochem Photobiol 2006;82:1097–102.

Gantz I, Konda Y, Tashiro T, Shimoto Y, Miwa H, Munzert G, et al. Molecular cloning of a novel melanocortin receptor. J Biol Chem 1993;268:8246–50.

Hatta N, Dixon C, Ray AJ, Phillips SR, Cunliffe WJ, Dale M, et al. Expression, candidate gene, and population studies of the melanocortin 5 receptor. J Invest Dermatol 2001;116:564–70.

Hattori K, Nishikawa M, Watcharanurak K, Ikoma A, Kabashima K, Toyota H, et al. Sustained exogenous expression of therapeutic levels of IFN-γ ameliorates atopic dermatitis in NC/Nga mice via Th1 polarization. J Immunol 2010;184:2729–35.

Herrmann T, Van der Hoeven F, Gröne HJ, Stewart AF, Langbein L, Kaiser I, et al. Mice with targeted disruption of the fatty acid transport protein 4 (Fatp 4, Slc27a4) gene show features of lethal restrictive dermopathy. J Cell Biol 2003;161:1105–15.

Imokawa G, Ishida K. Role of ceramide in the barrier function of the stratum corneum, implications for the pathogenesis of atopic dermatitis. J Clin Exp Dermatol Res 2014;5:1–12.

Jozic I, Stojadinovic O, Kirsner RSF, Tomic-Canic M. Skin under the (Spot)-light: cross-talk with the central hypothalamic-pituitary-adrenal (HPA) axis. J Invest Dermatol 2015;135:1469–71.

Lee DJ, Preble J, Lee S, Foster CS, Taylor AW. MC5r and A2Ar deficiencies during experimental autoimmune uveitis identifies distinct T cell polarization programs and a biphasic regulatory response. Sci Rep 2016;6:37790.

Lee DJ, Taylor AW. Both MC5r and A2Ar are required for protective regulatory immunity in the spleen of post-experimental autoimmune uveitis in mice. J Immunol 2013;191:4103–11.

Lovászi M, Szegedi A, Zouboulis CC, Törőcsik D. Sebaceous-immunobiology is orchestrated by sebum lipids. Dermatoendocrinol 2017;9:e1375636.

Muhammad F, Wang D, Montieth A, Lee S, Preble J, Foster CS, et al. PD-1^{+} melanocortin receptor dependent-Treg cells prevent autoimmune disease. Sci Rep 2019;9:16941.

O'Garra A, Vieira PL, Vieira P, Goldfeld AE. IL-10–producing and naturally occurring CD4^{+} Tregs: limiting collateral damage. J Clin Invest 2004;114:1372–8.

Oda T, Tachimoto H, Kishi M, Kaga T, Ichihashi M. Effect of oral intake of ceramide-containing acetic acid Bcteria on skin barrier function. J Anti Aging Med 2010;7:50–4.

Ponec M, Boelsma E, Weerheim A, Mulder A, Bouwstra J, Mommaas M. Lipid and ultrastructural characterization of reconstructed skin models. Int J Pharm 2000;203:211–25.

Reynier M, Allart S, Gaspard E, Moga A, Goudounèche D, Serre G, et al. Rab11a is essential for lamellar body biogenesis in the human epidermis. J Invest Dermatol 2016;136:1199–209.

Scaletta LJ, Occhino JC, MacCallum DK, Lillie JH. Isolation and immunologic identification of basement membrane zone antigens from human skin. Lab Invest 1978;39:1–9.

Segre JA, Bauer C, Fuchs E. Klf4 is a transcription factor required for establishing the barrier function of the skin. Nat Genet 1999;22:356–60.

Simamura E, Shimada H, Shoji H, Otani H, Hatta T. Effects of melanocortins on fetal development. Congenit Anom (Kyoto) 2011;51:47–54.

Skobowiat C, Dowdy JC, Sayre RM, Tuckey RC, Slominski A. Cutaneous hypothalamic-pituitary-adrenal axis homolog: regulation by ultraviolet radiation. Am J Physiol Endocrinol Metab 2011;301:E484–93.

Thiboutot D, Sivarajah A, Gilliland K, Cong Z, Clawson G. The melanocortin 5 receptor is expressed in human sebaceous glands and rat preputial cells. J Invest Dermatol 2000;115:614–9.

Uchida Y, Houben E, Park K, Douangpanya S, Lee YM, Wu BX, et al. Hydrolytic pathway protects against ceramide-induced apoptosis in keratinocytes exposed to UVB. J Invest Dermatol 2010;130:2472–80.

Uchida Y, Nardo AD, Collins V, Elias PM, Holleran WM. De novo ceramide synthesis participates in the ultraviolet B irradiation-induced apoptosis in undifferentiated cultured human keratinocytes. J Invest Dermatol 2003;120:662–9.

van der Kraan M, Adan RA, Entwistle ML, Gispen WH, Burbach JP, Tatro JB. Expression of melanocortin-5 receptor in secretory epithelia supports a functional role in exocrine and endocrine glands. Endocrinology 1998;139:2348–55.

Wertz P. Epidermal lamellar granules. Skin Pharmacol Physiol 2018;31: 262–8.

Yamamoto H, Hattori M, Chamulitrat W, Ohno Y, Kihara A. Skin permeability barrier formation by the ichthyosis-causative gene FATP4 through formation of the barrier lipid ω-O-acylceramide. Proc Natl Acad Sci USA 2020;117:2914–22.

Zhang L, Li WH, Anthonavage M, Eisinger M. Melanocortin-5 receptor: a marker of human sebocyte differentiation. Peptides 2006;27:413–20.

Zhang L, Li WH, Anthonavage M, Pappas A, Rossetti D, Cavender D, et al. Melanocortin-5 receptor and sebogenesis. Eur J Pharmacol 2011;660: 202–6.

Zhu M, Wang M, Chen Y, Zhang C. Pharmacological modulation of two melanocortin-5 receptors by MRAP2 proteins in zebrafish. J Mol Endocrinol 2019;62:27–36.